Title	Elastic, anelastic, and piezoelectric coefficients of Langasite : Resonance ultrasound spectroscopy with laser-doppler interferometry
Author(s)	Ogi, Hirotsugu; Nakamura, Nobutomo; Sato, Keiji et al.
Citation	IEEE Transactions on Ultrasonics, Ferroelectrics, and Frequency Control. 2003, 50(5), p. 553-560
Version Type	AM
URL	https://hdl.handle.net/11094/84144
rights	© 2003 IEEE. Personal use of this material is permitted. Permission from IEEE must be obtained for all other uses, in any current or future media, including reprinting/republishing this material for advertising or promotional purposes, creating new collective works, for resale or redistribution to servers or lists, or reuse of any copyrighted component of this work in other works.
Note	

Elastic, Anelastic, and Piezoelectric Coefficients of Langasite (La$_3$Ga$_5$SiO$_{14}$): Resonance Ultrasound Spectroscopy with Laser-Doppler Interferometry

Hirotsugu Ogi, Nobutomo Nakamura, Keiji Sato, and Masahiko Hirao
Graduate School of Engineering Science, Osaka University,
Machikaneyama 1-3, Toyonaka, Osaka 560-8531, Japan

Satoshi Uda
Microelectronics Laboratories, Mitsubishi Materials Corp.,
Yokoze, Chichibu, Saitama 368-8503, Japan

ABSTRACT - This paper presents advanced techniques to determine all independent elastic-stiffness coefficients C_{ij}, the associated internal friction Q_{ij}^{-1}, and piezoelectric coefficients e_{ij} of monocrystal langasite (La$_3$Ga$_5$SiO$_{14}$) using a single rectangular parallelepiped specimen. Langasite's crystal structure belongs to the trigonal system with point group 32, thus six independent C_{ij}, two e_{ij}, and two dielectric coefficients ε_{ij}. All of the elastic and piezoelectric coefficients affect the mechanical resonance frequencies of the solid specimen, and measuring them very accurately permits one to determine the C_{ij} and e_{ij} with known density, dimensions, and ε_{ij}. We developed a piezoelectric tripod to support the specimen upward and measured the free-vibration resonance frequencies with minimum load from its own weight. This weak and stable acoustic coupling ensures high accuracy of the frequency measurement better than 10^{-5}, being enough to determine the reliable coefficients. Our C_{ij} fall in the range of results measured with previous (conventional) methods. Our e_{11} is smaller than the reported values by 1.2-13%, and e_{14} is larger than those by 44-97%. For the internal friction measurement, we used a solenoid coil to vibrate the specimen without any contact. The longitudinal-wave internal friction considerably exceeds the shear-wave internal friction, which can be interpreted as phonon-phonon interactions.

I. INTRODUCTION

Langasite ($La_3Ga_5SiO_{14}$) attracts many researchers because of its large piezoelectric coefficients and less-temperature-dependent elastic constants.   These properties are especially suitable for surface-acoustic-wave (SAW) filters [1-8] and langasite is replacing quartz in wide variety of electric devices.   Langasite belongs to crystals with 32 point-group symmetry that show six independent elastic-stiffness coefficients C_{ij}, two piezoelectric coefficients e_{ij}, and two dielectric coefficients ε_{ij}. Besides, six independent internal friction Q_{ij}^{-1} will exist.   Optimization of an electric device requires a complete set of the material coefficients and significant efforts have been made for measuring them [2-8].   The dielectric coefficients are available from low-frequency capacitance measurements [9], but measuring all of the elastic and piezoelectric coefficients presents a formidable task as demonstrated by Smith and Welsh [10].   Conventional methods used in previous studies [2-9] involve many independent measurements on many crystals in many orientations; the pulse-echo measurements or rod-resonance measurements coupled with the resonance-antiresonance measurements of electric impedance.   Then, one must solve a set of labyrinthine equations. Various errors thus easily occur, being associated with the use of different specimens, crystal's misorientation, resonance frequency shifts by attaching electrodes, and so on.   Concerning the internal friction tensor Q_{ij}^{-1} of langasite, only one study appears by Ledbetter et al. [11].

Here, we propose an advanced methodology that determines all the elastic, anelastic, and piezoelectric coefficients from a single rectangular-parallelepiped specimen.   We note that the mechanical resonance frequencies of a piezoelectric solid depend on the C_{ij} and e_{ij}, and that resonant ultrasound spectroscopy (RUS) can detect them, from which an inverse calculation yields the needed coefficients.   In the past, this approach was used to determine only the C_{ij} of metals [12-15], composites [16-18], intermetallic compounds [19].   For quartz, Ohno [20] determined the C_{ij}, neglecting the e_{ij} and ε_{ij}.   For lithium niobate (showing much larger piezoelectric coefficients than quartz), Ledbetter and Dunn [21] found that e_{ij} and ε_{ij} considerably affect the resonance frequencies and suggested that accurate frequency measurements would deduce the e_{ij} as well.   For langasite, the e_{ij}'s contribution to the frequencies is in the order of 10^{-2} at most.   To deduce them accurately, the resonance- frequency measurements must be done with accuracy of 10^{-4} or better.   Even more important is the mode matching between the observed and calculated resonances.   Mode mismatch is fatal to obtain these less contributing coefficients.   Therefore, obtaining the reliable e_{ij} along with

the C_{ij} requires precise frequency measurements and correct mode identification. We realize this by using a piezoelectric tripod to detect *free* oscillation of the specimen and by incorporating laser interferometry into the resonance measurement to scan the surface displacement for identifying the vibrating modes. For internal friction, we used a contactless free-decay method to deduce Q_{ij}^{-1}.

II. MATERIAL

We used five oriented rectangular parallelepiped crystals (*specimen A* to *E*). Using Archimedes's method and distilled water as a standard, we determined the mass density ρ. Their dimensions and mass density are given in Table I. The material coefficients in contracted notation can be written as:

$$[C_{ij}] = \begin{bmatrix} C_{11} & C_{12} & C_{13} & C_{14} & 0 & 0 \\ C_{12} & C_{11} & C_{13} & -C_{14} & 0 & 0 \\ C_{13} & C_{13} & C_{33} & 0 & 0 & 0 \\ C_{14} & -C_{14} & 0 & C_{44} & 0 & 0 \\ 0 & 0 & 0 & 0 & C_{44} & C_{14} \\ 0 & 0 & 0 & 0 & C_{14} & (C_{11}-C_{12})/2 \end{bmatrix},$$

$$[e_{ij}] = \begin{bmatrix} e_{11} & -e_{11} & 0 & e_{14} & 0 & 0 \\ 0 & 0 & 0 & 0 & -e_{14} & -e_{11} \\ 0 & 0 & 0 & 0 & 0 & 0 \end{bmatrix},$$

and

$$[\varepsilon_{ij}] = \begin{bmatrix} \varepsilon_{11} & 0 & 0 \\ 0 & \varepsilon_{11} & 0 \\ 0 & 0 & \varepsilon_{33} \end{bmatrix}.$$

III. MEASUREMENT

A. RUS/Laser technique

RUS usually measures mechanical resonance frequencies of a solid specimen by sandwiching

it between two piezoelectric transducers for the transmission and detection of acoustic vibration. This setup restricts the specimen's displacements and raises the frequencies from those at ideal *free* vibrations.   To minimize this influence, we use a piezoelectric tripod consisting of two pinducers for generation and detection of vibration, and one only for support (Fig. 1).   No external force was applied to the specimen, except for the specimen weight, nor any coupling agent was used.   A frequency scan detected all the resonance peaks in a frequency band as shown in Fig. 2.   We measured them at constant temperature of 30±0.02°C three times for each specimen.   Owing to the weak coupling, reproducibility among the independent measurements was better than 10^{-5}.

After finishing the series of measurements (including the internal-friction measurement described below), we deposited 100-nm aluminum film on a specimen surface for mode identification with laser interferometry.   (This deposition was needed because langasite is a transparent material.)   A He-Ne laser beam was focused on the vibrating specimen surface with 15μm focal diameter.   The reflected beam entered the Doppler interferometer, which detected the normal component of the velocity at the focal point.   The velocity was easily converted into the normal displacement because of harmonic oscillation.   Depositing aluminum shifted so slightly the resonance frequencies that the modes are clearly identified after the deposition.

B. Dynamic electromagnetic filed technique

Not significant, but the piezoelectric tripod still causes energy leakage into the touching pinducers and as-measured internal friction contains a background.   The best way to measure internal friction is to introduce vibration sources inside the specimen in a noncontact way using the piezoelectric effect of langasite itself.   We used a solenoid coil to excite and detect the free vibrations by means of the dynamic electromagnetic field.   Johnson [22] first adopted this approach for studying temperature dependence of internal friction of langatate ($La_3Ga_{5.5}Ta_{0.5}O_{14}$), an isomorph of langasite, but not for the internal-friction tensor Q_{ij}^{-1}.

Figure 3 shows our measurement setup.   The specimen was inserted in a solenoid coil, which was loose and never constrained the specimen.   We put a thin polymer sheet between the specimen and coil wires.   The specimen and sheet are in contact at a few points, but because of the large acoustic-impedance mismatch and no applied force, they are acoustically noncontacting.   We drove the coil with high-power rf bursts to induce oscillating electric field near the specimen surfaces and to excite the free vibration through the converse piezoelectric effect.   After the excitation, the same

coil received the vibration through the piezoelectric effect.   We processed the received signals with an analog superheterodyne spectrometer to extract the signal amplitude at the tone-bursts frequency [23].   A frequency scan provided the resonance peaks (Fig. 2).   We obtained the amplitude decay of vibration after exciting the coil at a resonance frequency and determined the attenuation coefficient α, which leads to internal friction via $Q^{-1}=\alpha/\pi f$.   Figure 4 exemplifies the measured amplitude decay and a fitted exponential function.   Due to the frequency limit of our instrument, we measured internal friction of the smaller specimens *A* to *C*.

We did not utilize this noncontact method to determine the C_{ij} and e_{ij} through the resonance frequencies because of much fewer peaks than those measured by the piezoelectric tripod.   For example, only A_g vibration modes were observed in Fig. 2.   The detectable modes depend on the geometrical relationship between the crystal orientation and solenoid coil, that is, on the electric-field direction.   Other configurations detected only B_g vibration modes.   But, we failed to detect A_u and B_u modes with the solenoid coil.   (Mode notation will be shown in the next section.)

IV. INVERSE CALCULATION

A. C_{ij} and e_{ij}

The governing equations showing the interconnection between elastic and electric properties are

$$T_{ij} = C_{ijkl}S_{kl} - e_{kij}E_k \quad , \tag{1}$$

$$D_i = e_{ikl}S_{kl} + \varepsilon_{ij}E_j \quad , \tag{2}$$

$$S_{kl} = \frac{\partial u_k}{\partial x_l} + \frac{\partial u_l}{\partial x_k}, \tag{3}$$

where T_{ij} is a component of the stress tensor. E_i, D_i, and u_i denote electric field, electric flux density, and displacement along the x_i axis, respectively.   The electric field can be divided into a rotational component and an irrotational component (or quasistatic field).   In the megahertz-frequency region, the rotation component is negligible and the quasistatic electric field dominates, which is expressed by the electric potential ϕ [24]

$$E_k = -\frac{\partial \phi}{\partial x_k} \quad . \tag{4}$$

(As will be shown in Fig. 6, this quasistatic approximation actually causes trivial errors in the resonance frequency calculation.)   Substituting Eqs.(1)-(4) into the equation of motion

$$-\rho\omega^2 u_i = \frac{\partial T_{ij}}{\partial x_j}, \tag{5}$$

with the boundary conditions for the stresses and electric field would lead to the free-vibration resonance frequencies ω of the system.   However, analytical solutions for the displacements and electric potential are unavailable for rectangular-parallelepiped piezoelectric specimens.   Eer Nisse [25] then derived the Lagrangian of a vibrating piezoelectric material as

$$L = \frac{1}{2}\int_v \left(S_{ij}C_{ijkl}S_{kl} - \frac{\partial\phi}{\partial x_m}\varepsilon_{mn}\frac{\partial\phi}{\partial x_n} + 2\frac{\partial\phi}{\partial x_m}e_{mkl}S_{kl} - \rho\omega^2 u_i u_i \right)dV. \tag{6}$$

The stationary point of the Lagrangian gives the resonance modes (δL=0).   Ohno [20] used approximation for the displacements and electric potential in terms of linear combinations of the basis functions ψ consisting of the normalized Legendre polynomials:

$$u_i(x_1,x_2,x_3) = \sum_k a_k^i \Psi_k^i(x_1,x_2,x_3), \tag{7}$$

$$\phi(x_1,x_2,x_3) = \sum_k a_k^\phi \Psi_k^\phi(x_1,x_2,x_3). \tag{8}$$

Here

$$\Psi_k(x_1,x_2,x_3) = \sqrt{\frac{8}{L_1 L_2 L_3}}\overline{P}_l(2x_1/L_1)\overline{P}_m(2x_2/L_2)\overline{P}_n(2x_3/L_3). \tag{9}$$

$\overline{P}_\lambda$ denotes the normalized Legendre polynomial of degree λ and L_i denotes the edge length along the x_i axis of the rectangular parallelepiped.   The Lagrangian minimization with a Rayleigh-Ritz approach [12, 13] determines the resonance frequencies together with the associated sets of expansion coefficients a_k^i.   An oriented rectangular-parallelepiped crystal with 32 point-group symmetry has four vibration groups labeled as A_g, B_g, A_u, and B_u, according to the deformation symmetry as tabulated by Ohno [20].   Choosing proper combinations of basis functions thus reduces the calculation time.   While following Ohno's calculation (forward calculation), we implemented a least-squares-fitting procedure for the calculated and measured resonance frequencies to deduce the C_{ij} and e_{ij}.

In this inverse-calculation, comparison of the measurements with the calculations must be made on correctly the same resonance mode.   (Otherwise, resultant material coefficients are physically

meaningless.)   However, this has never been an easy task and mode mismatches easily occurred

because nearly one hundred resonance peaks are observed and some of them appear at very close

frequencies.   To overcome this difficulty, we pay a special attention to the expansion coefficients

a_k^i.   They tell us the displacement distribution on a specimen surface, a *fingerprint* of an individual

mode.   Thus, comparison between the measured and computed displacement distributions leads us

to unmistakable mode identification.

One cannot separately determine the e_{ij} and ε_{ij} from mechanical spectroscopy because their

ratios affect the resonance frequencies.   Fortunately, the ε_{ij} can be obtained by the capacitance

measurements with good accuracy.   Actually, several researchers reached close ε_{ij} within a 2%

range, while there are a lot of discrepancies for other coefficients (see Table II).   For this reason, we

fixed the ε_{ij} at averaged values over the previous studies.

B. Q_{ij}^{-1}

We neglect the piezoelectric effect for the calculation of internal friction tensor because their

contributions to the resonance vibration are much smaller than those of the elastic stiffness

coefficients.   Internal friction Q_{ij}^{-1} can be considered as the ratio of imaginary-to-real part of the

complex elastic stiffness $\widetilde{C}_{ij}$ [14], or

$$\widetilde{C}_{ij} = C_{ij}(1 + jQ_{ij}^{-1}).\tag{10}$$

Determination of all independent C_{ij} and their companion internal friction Q_{ij}^{-1} permits one to predict

unmeasurable mechanical loss of any ultrasonic modes and then to select less-lossy mode,

propagation direction, and surface orientation for designing acoustic devices.   Calculation of the

internal-friction tensor is based on a reasonable assumption that the square of the complex frequency

can be expressed by a linear combination of complex elastic-stiffness coefficients:

$$\widetilde{f}_p^{\,2} = \sum_q \frac{\partial f_p^2}{\partial C_q} \widetilde{C}_q = \sum_q 2f_p b_{pq} C_q \left(1 + jQ_q^{-1}\right),\tag{11}$$

Here, $\widetilde{f}_p$ denotes the complex frequency of the pth resonance and q denotes the matrix-notation

subscripts (i.e. q=11, 12, 13, …). $b_{pq}(=\partial f_p/\partial C_q)$ means the sensitivity of the elastic stiffness C_q to

the resonance frequency f_p, which is obtainable in the inverse calculation [13]. On the other hand, we can define a particular modulus C_p and internal friction Q_p^{-1} constructing the complex resonance frequency as

$$\tilde{f}_p^{\,2} = \text{const.}\tilde{C}_p = \text{const.}C_p\left(1+jQ_p^{-1}\right) = f_p^2\left(1+jQ_p^{-1}\right). \tag{12}$$

Comparison of Eq. (11) with Eq. (12) leads to

$$Q_p^{-1} = \frac{2\sum_q b_{pq}C_qQ_q^{-1}}{f_p} \quad \text{and} \quad \frac{2\sum_q b_{pq}C_q}{f_p} = 1. \tag{13}$$

The quantities f_p and Q_p^{-1} (peak width) corresponds to the measured resonance frequencies and internal friction, respectively, and b_{pq} are obtainable as a result of the inverse calculation. Then, we can deduce the Q_q^{-1} ($=Q_{ij}^{-1}$) with a standard least-squares procedure.

V. RESULTS

Figure 5 shows examples of measured and computed displacement figures on a vibrating crystal surface. Excellent agreement allowed us to make unambiguous mode identification. We identified more than sixty peaks for each specimen and entered them into the inverse calculation. Figure 6 plots the differences between the measured and calculated resonance frequencies after the inverse calculation for all specimens. It also includes plots from purely elastic calculation neglecting e_{ij} and ε_{ij}. The piezoelectric effect raises the frequencies, that is, piezoelectric stiffening. Correlation coefficient between the measurements and calculations was 0.99999 and rms error between them was 0.065%. This agreement indicates the validity of the quasistatic approximation made in the analysis. Table I shows the determined elastic and piezoelectric coefficients. Despite various specimen dimensions, the resulting coefficients are close with each other. Averages over the five specimens are our final results, which are compared with previously reported values in Table II.

Figure 7 shows the measured internal friction (Q_p^{-1}).   The measurements by the piezoelectric tripod exceeded those by the contactless method using the solenoid coil, especially at lower frequencies. This implies that the RUS internal friction contains energy loss caused by contacting. In Table II, we show the six components of Q_{ij}^{-1}, which were deduced from all measurements for the three specimens by the solenoid coil.

V. DISCUSSION

A. C_{ij} and e_{ij}

Possible errors arising in the present method are (i) frequency-measurement error (~0.001%), (ii) dimensions and density error (<0.02%), (iii) crystal's misorientation error (less than 1°), and (iv) calculation error (<0.065%).   Among them, we consider that the last issue dominates the accuracy of the resulting coefficients.   The calculation error originates from the approximation for the displacements and electric potential in the inverse calculation.   (Increasing the number of basis functions can reduce this error.)   Therefore, a coefficient that contributes less to the resonance frequencies than the calculation error would not be determined on a rigorous basis.   We calculated the normalized contributions of the coefficients to the resonance frequencies.   Among all the coefficients, e_{14} showed the smallest contribution, 0.45% on average. (This is probably the main reason that previously reported e_{14} widely ranges.)   However, this is still larger than the calculation error by a factor 7, indicating that reliable coefficients are obtainable.   Using the contribution and the calculation error for each resonance mode, we estimated possible errors included in the resulting coefficients.   The largest error occurs in e_{14} by 4%, which is smaller than the standard deviation among the five specimens (~7%) in Table I.   Thus, differences of the resulting coefficients among the five specimens occur due to the difference of the crystal.

It has been pointed out that such an inverse calculation is much affected by the initial guess to start the iteration calculations, especially when the modes are not identified [12, 13, 15].   However, because we can correctly identify the observed modes by referring to the displacement figures, the resulting coefficients are insensitive to the initial guess.   Indeed, we always reached exactly the same answer from any previously reported values as an initial guess.   Furthermore, the inverse calculation provided the correct answer even with an unreasonable initial guess, listed in the caption of Fig. 5.   This is because the displacement-distribution patterns were hardly affected by the

material coefficients as demonstrated in Fig. 5.   They are unique for individual modes like fingerprints.   On the other hand, we failed to obtain the true values without referring to the displacement figures, even beginning with a good initial guess by Kaminskii et al.[2].   Thus, the correct mode identification is the key for the successful determination of the material coefficients.

Concerning the elastic-stiffness coefficients, our results fall within the previous error limits. For the piezoelectric coefficients, however, our results considerably differ from the widely ranging previous results; e_{11} is smaller by 1.2-13% and e_{14} is larger by 44-97% than the existing results.   We are confident about our results, because we removed the error sources of the conventional measurements; (i) coupling agent and excess load for transduction, (ii) electrodes on the specimen surfaces, and (iii) use of many specimens oriented in various directions.   Moreover, the pulse-echo measurements are vulnerable to noises and waveform change caused by many factors.

B. Q_{ij}^{-1}

Obviously, Q_{11}^{-1} and Q_{33}^{-1} exceed Q_{44}^{-1} and Q_{66}^{-1} by a factor about 5.   We repeated the determination of Q_{ij}^{-1} three times and found that they varied by 20% at most.   Thus, this difference is meaningful and indicates that longitudinal-wave attenuation is larger than shear-wave attenuation, a contrary trend to metals where dislocations' anelastic movement causes larger shear-wave Q^{-1} [14, 15].

Possible origin of internal friction of such a brittle material is phonon-phonon interactions. Acoustic waves break an equilibrium state of phonons due to the lattice anharmonicity.   The scattered thermal-mode phonons subsequently equilibrate by interacting with a low-frequency-mode (acoustic) phonon and other thermal-mode phonons, during which energy loss arises.   Such energy loss can be expressed by the relaxation time τ of an acoustic phonon to relax to a thermal phonon with angular frequency of the acoustic wave ω (Akhieser result) [26].   At room temperature and in the kilohertz frequency region ($\omega\tau\ll 1$), it reduces

$$Q_{phon}^{-1} = \text{const.}\omega\tau, \tag{14}$$

where C is a constant depending on the mass density, sound velocity, and the lattice anharmonicity. This theory agreed with measurements of germanium, quartz, and silicon as summarized in Mason's thesis [26].   Especially, germanium shows the longitudinal/shear-modes internal-friction ratio about 5, very close to ours on langasite.   Usually, the thermal relaxation time for longitudinal waves is

about twice that for shear waves because of the difference of the associated volume change [26]. Our Q_{ij}^{-1} then can be interpreted as phonon-phonon interactions.

5. CONCLUSIONS

(1) We developed the RUS/Laser hybrid technique to perform the simultaneous determination of the elastic and piezoelectric coefficients of langasite from a single specimen. Accuracy of the frequency measurement was better than 0.001%. We succeeded in correctly identifying all of the observed resonance peaks by measuring the displacement distributions on a surface using laser-Doppler interferometry. The measured coefficients are independent of the specimen dimensions.

(2) Our elastic coefficients are consistent with those reported previously using conventional measurement methods. Our piezoelectric coefficients were considerably different from those reported in the past.

(3) Our elastic and piezoelectric coefficients are insensitive to the initial guess for iteration owing to exact mode identification.

(4) We measured internal friction using a contactless free-decay method and deduced the internal friction tensor. Longitudinal-wave internal friction was larger than shear-wave internal friction by a factor about 5, which was interpreted as phonon-phonon interactions.

REFERENCES

1 T. Sato, M. Murota, and Y. Shimizu, "Characteristics of Rayleigh and Leaky Surface Acoustic Wave Propagating on a $La_3Ga_5SiO_{14}$ Substrate," Jpn. J. Appl. Phys., vol. 37, pp. 2914-2917, 1998.   (Many other studies appear in 1998-2000 IEEE Ultrasonic Symposium Proceedings.)

2 A. Kaminskii, I. Silvestrova, S. Sarkisov, and G. Denisenko, "Investigation of Trigonal $(La_{1-x}Nd_x)_3Ga_5SiO_{14}$ Crystals," Phys. Stat. Sol. (a), vol. 80, pp. 607-620, 1983.

3 A. Ilyaev, B. Umarov, L. Shabanova, and M. Dubovik, "Temperature Dependence of Electromechanical Properties of LGS Crystals," Phys. Stat. Sol. (a), vol. 98, pp. K109-K114, 1986.

4 I. Sil'vestrova, Y. Pisarevskii, P. Senyushchenkov, and A. Krupnyi, "Temperature Dependence of the Properties of $La_3Ga_5SiO_{14}$ Single Crystal," Sov. Phys. Solid State, vol. 28, pp. 1613-1614, 1986; through J. Gualtieri, J. Kosinski, and A. Ballato, "Piezoelectric Materials for Acoustic Wave Applications," IEEE Trans. Ultrason. Ferroelect. Freq. Contr., vol. 41, pp. 53-59, 1994.

5 S. Sakharov, P. Senushencov, A. Medvedev and Yu. Pisarevsk, "New Data on Temperature Stability and Acoustical Losses of Langasite Crystals," Proc. IEEE Freq. Contr. Symp., pp. 647-652, 1995.

6 K. Inoue and K. Sato, "Propagation Characteristics of Surface Acoustic Waves on Langasite," Jpn. J. Appl. Phys., vol. 37, pp. 2909-2913, 1998.

7 A. Bungo, C. Jian, K. Yamaguchi, Y. Sawada, S. Uda, and Y. Pisarevsky, "Analysis of Surface Acoustic Wave Properties of the Rotated Y-Cut Langasite Substrate," Jpn. J. Appl. Phys., vol. 38, pp. 3239-3243, 1999.

8 D. Malocha, M. Cunha, E. Adler, R. Smythe, S. Frederick, M. Chou, R. Helmbold, and Y. Zhou, "Recent Measurements of Material Constants versus Temperature for Langatate, Langanite and Langasite," 2000 IEEE/EIA Int. Freq. Contr. Symp. and Exhib., pp. 200-205, 2000.

9 IEEE Standard on Piezoelectricity in IEEE Transactions on Sonics and Ultrasonics, vol. SU-31, ANSI/IEEE Std 176-1978, The IEEE Inc., 1979.

10 R. Smith and F. Welsh, "Temperature Dependence of the Elastic, Piezoelectric, and Dielectric Constants of Lithium Tantalate and Lithium Niobate," J. Appl. Phys., vol. 42, pp. 2219-2230, 1971.

11 H. Ledbetter, S. Kim, and M. Lei, personal communication, 2002.

12 I. Ohno, "Free Vibration of a Rectangular Parallelepiped Crystal and Its Application to Determination of Elastic Constants of Orthorhombic Crystals," J. Phys. Earth, vol. 24, pp. 355-379, 1976.

13 A. Migliori, J. Sarrao, W. Visscher, T. Bell, M. Lei, Z. Fisk, and R. Leisure, "Resonant Ultrasonic Spectroscopy Techniques for Measurement of the Elastic Moduli of Solids," Physica B, vol. 183, pp. 1-24 1993.

14 H. Ledbetter, C. Fortunko, and P. Heyliger, "Elastic Constants and Internal Friction of Polycrystalline

Copper," J. Mater. Res., vol. 10, pp. 1352-1353, 1995.

15 H. Ogi, H. Ledbetter, S. Kim, and M. Hirao: "Contactless Mode-Selective Resonance Ultrasound Spectroscopy: Electromagnetic Acoustic Resonance," J. Acoust. Soc. Am., vol. 106, pp. 660-665, 1999.

16 H. Ledbetter, C. Fortunko, and P. Heyliger, "Orthotropic Elastic Constants of a Boron-Aluminum Fiber-Reinforced Composite: An Acoustic-Resonance-Spectroscopy Study," J. Appl. Phys., vol. 78, pp. 1542-1546, 1995.

17 H.Ogi, K. Takashima, H. Ledbetter, M. Dunn, G. Shimoike, M. Hirao, and P. Bowen: "Elastic Constants and Internal Friction of an SiC-Fiber-Reinforced Ti-Alloy-Matrix Crossply Composite: Measurement and Theory," Acta Materialia, vol. 47, pp. 2787-2796, 1999.

18 H. Ogi, M. Dunn, K. Takashima, and H. Ledbetter: "Elastic Properties of a SiC_f/Ti Unidirectional Composite: Acoustic Resonance Measurements and Micromechanics Predictions," J. Appl. Phys., vol. 87, 2769-2774, 2000.

19 K. Tanaka and M. Koiwa, "Single-Crystal Elastic Constants of Intermetallic Compounds," Intermetallics, vol. 4, pp. S29-S39, 1996.

20 I. Ohno, "Rectangular Parallelepiped Resonance Method for Piezoelectric Crystals and Elastic Constants of Alpha-Quartz," Phys. Chem. Minerals, vol. 17, pp. 371-378, 1990.

21 M. Dunn, H. Ledbetter, and P. Heyliger, "Free Vibration of Piezoelectric Crystals: Application to the Determination of Elastic and Piezoelectric Constants," in Engineering Mechanics, ASME, Washington, pp. 758-761, 1995.

22 W. Johnson, S. Kim, and D. Lauria, "Anelastic Loss in Langatate," in Proc. IEEE/EIA Int. Freq. Contr. Symp. and Exhib., pp. 186-190, 2000.

23 M.Hirao, H.Ogi, and H.Fukuoka, "Resonance EMAT System for Acoustoelastic Stress Evaluation in Sheet Metals," Rev. Sci. Instrum., vol. 64, pp. 3198-3205, 1993.

24 B. A. Auld, *Acoustic Fields and Waves in Solids*. vol. 1, New York: Wiley-Interscience, 1973, p.298.

25 EP Eer Nisse, "Variational Method for Electroelastic Vibration Analysis," IEEE Trans Sonics Ultrasonics, vol. SU-14, pp. 153-160, 1967.

26 W. Mason, "Effect of Impurities and Phonon Process on the Ultrasonic Attenuation of Germanium, Crystal Quartz, and Silicon," in *Physical Acoustics*, vol. IIIB, ed. W. Mason, New York: Academic, 1965, p. 254.

Table Captions

Table I   Dimensions L_i (mm), mass density ρ (10^3 kg/m^3), elastic-stiffness coefficients C_{ij} (GPa), and piezoelectric coefficients e_{ij} (C/m^2) of the five specimen crystals.

Table II Elastic-stiffness coefficients (GPa), piezoelectric coefficients (C/m^2), dielectric coefficients normalized by that in vacuum, and the internal friction tensor.

Table I

Dimensions L_i (mm), mass density ρ (10^3 kg/m^3), elastic-stiffness coefficients C_{ij} (GPa), and piezoelectric coefficients e_{ij} (C/m^2) of the five specimen crystals.

	Specimen A	Specimen B	Specimen C	Specimen D	Specimen E	average
L_1	2.966	2.97	8.032	10.024	9.965	——
L_2	3.745	5.768	9.814	10.043	10.048	——
L_3	4.012	4.012	6.022	13.764	14.406	——
ρ	5.723	5.730	5.713	5.731	5.723	5.724±0.007
C_{11}	189.4	190.6	190.4	188.7	188.7	189.5±0.9
C_{33}	261.0	262.8	263.3	263.2	262.6	262.6±0.9
C_{44}	53.35	53.95	53.37	53.50	53.33	53.50±0.26
C_{66}^{*}	42.10	42.28	42.10	42.05	41.94	42.09±0.12
C_{12}	105.2	106.0	106.2	104.6	104.8	105.4±0.7
C_{13}	96.80	97.12	98.28	96.77	96.83	97.16±0.64
C_{14}	14.19	14.47	14.28	14.18	14.11	14.25±0.14
e_{11}	-0.389	-0.387	-0.384	-0.405	-0.422	-0.397±0.02
e_{14}	0.183	0.208	0.22	0.209	0.194	0.203±0.01

* $C_{66}=(C_{11}-C_{12})/2$

Table II

Elastic-stiffness coefficients (GPa), piezoelectric coefficients (C/m^2), dielectric coefficients normalized by that in vacuum, and the internal friction tensor.

	present	Malocha et al. (2000)	Bungo et al. (1999)	Inoue & Sato(1998)	Sakharov et al. (1995)	Sil'vestrova et al. (1986)	Ilyaev et al. (1986)	Kaminskii et al. (1983)	present Q_{ij}^{-1} (10^{-4})
C_{11}	189.5	188.5	189	189.5	189.3	190.2	188.9	190.9	1.73
C_{33}	262.6	261.7	268	259.9	262.4	262.1	262.2	261.9	0.95
C_{44}	53.5	53.71	53.3	53.91	53.84	53.82	53.9	52.4	0.26
C_{66}	42.09	42.21	42.4	42.4	42.16	42	42.2	43.2	0.27
C_{13}	97.16	96.88	102	97.86	95.28	91.9	96.8	104.2	1.65
C_{14}	14.25	14.15	14.4	14.64	14.93	14.7	14.3	15.2	0.16
e_{11}	-0.397	-0.402	-0.438	-0.428	-0.431	——	-0.44	-0.45	——
e_{14}	0.203	0.13	0.104	0.114	0.108	——	0.07	0.077	——
ε_{11}	19.04[a]	19.62	19.06	19.07	18.97	——	18.86	18.99	——
ε_{33}	50.51[a]	49.41	51.06	50.3	52	49	49.1	49.32	——

[a] Averages of the previously reported values.

Figure Captions

Fig. 1.   Measurement setup of the RUS/Laser combination.

Fig. 2.   Resonance spectrum of *Specimen B* measured by the piezoelectric tripod and solenoid coil.

Fig. 3.   Measurement setup of the dynamic electromagnetic-field technique.

Fig. 4.   Free decay of the reverberating amplitude after the excitation.   Open circles denote measurements and solid line denotes the fitted exponential function.

Fig. 5.   Measured (left) and computed (middle and right) displacement figures on the *x* face of *Specimen E*.   The frequencies shown in parentheses are measured ones.   Bright area implies large displacement amplitude and black area zero amplitude, that is, nodal lines.   The maximum displacement amplitude was about 1nm.   In the computations, we used the coefficients taken from Kaminskii et al. [2] (middle) and C_{11}=200, C_{33}=220, C_{12}=70, C_{13}=80, C_{44}=47, and C_{14}=20 GPa; e_{11}=-0.5, e_{22}=0.01 C/m^2 (right), which are far away from the true values.

Fig. 6.   Differences between the measured (f_m) and calculated (f_c) resonance frequencies of the five specimens.   Taking the piezoelectric effect into consideration, the calculations agree with the measurements with 0.065% on average.   (▲△*A*, ▼▽*B*, ◆◇*C*, ■□*D*, ●○*E*)

Fig. 7.   Internal friction measured by the contactless free-decay method.   Open circles denotes the peak-width measurements by the piezoelectric tripod.
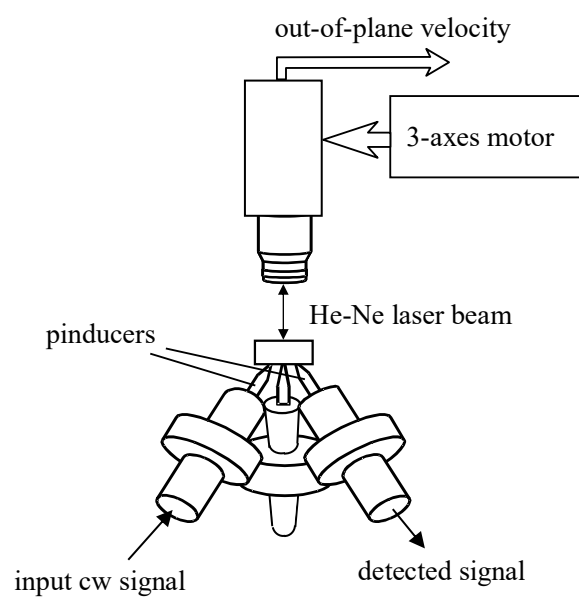
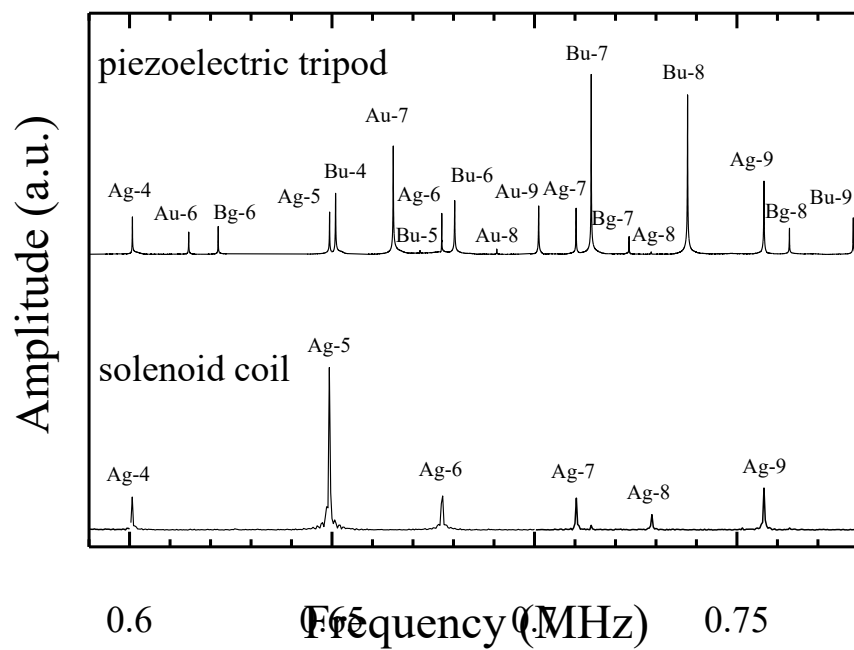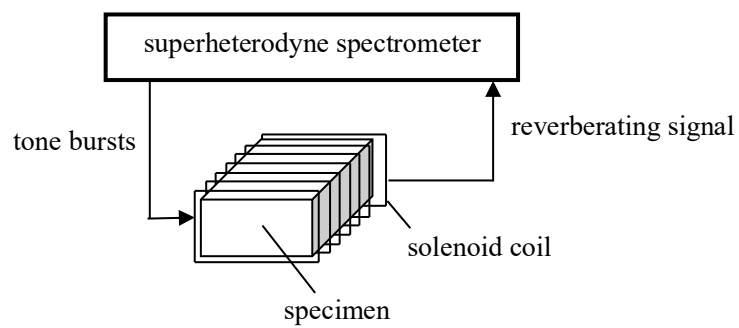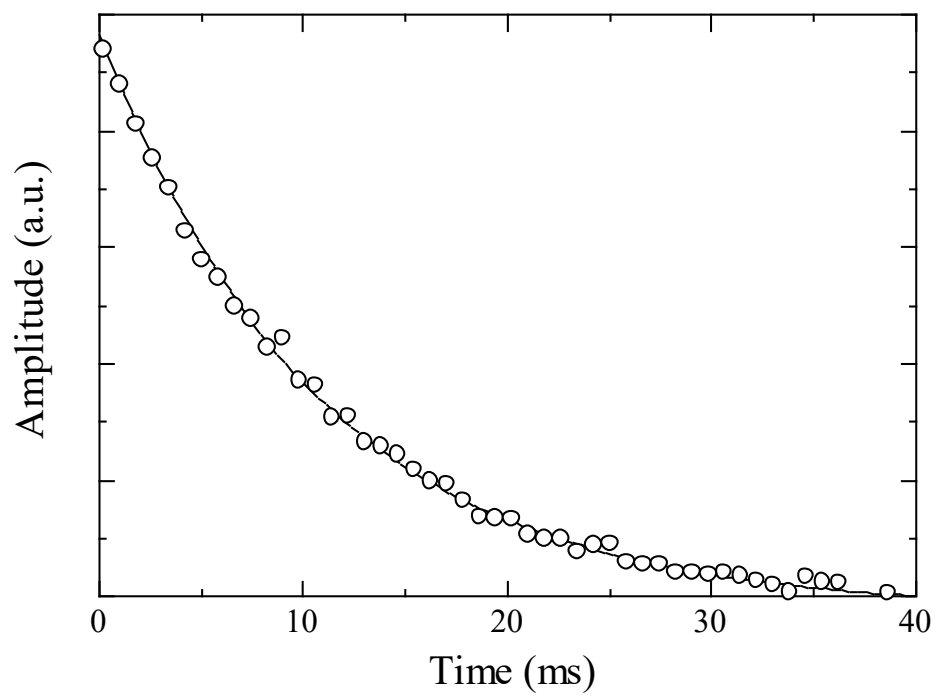out-of-plane velocity

3-axes motor

He-Ne laser beam

pinducers

input cw signal

detected signal

Fig. 1

Fig. 2

superheterodyne spectrometer

tone bursts

reverberating signal

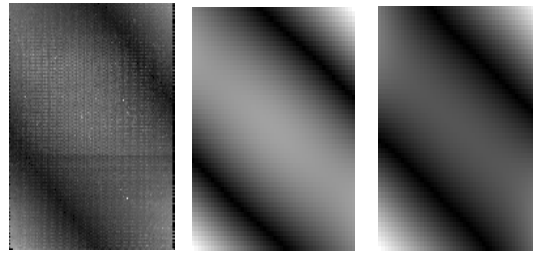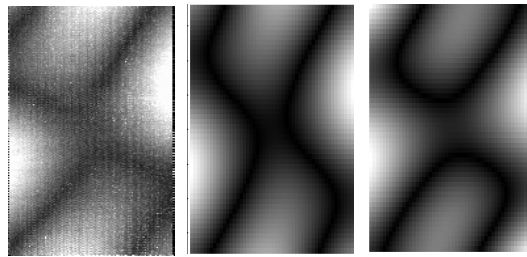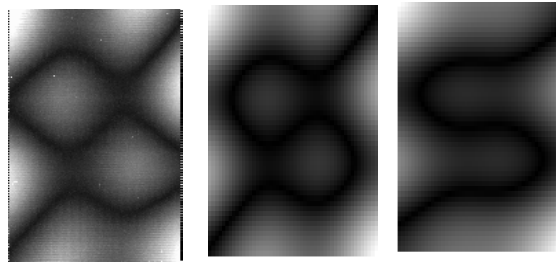solenoid coil

specimen

Fig. 3

Fig. 4

(a) A_g-4 (195 kHz)

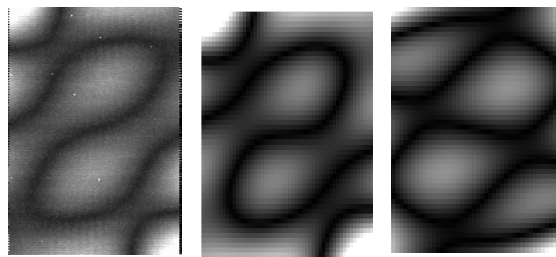(b) A_u-6 (240 kHz)

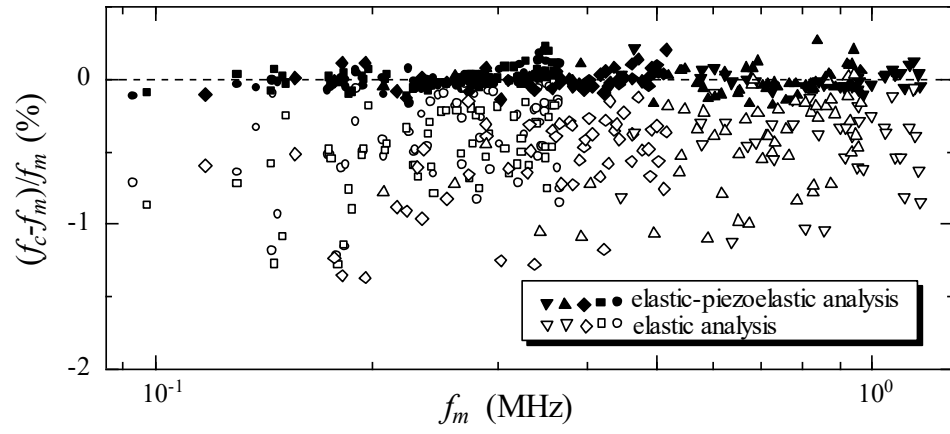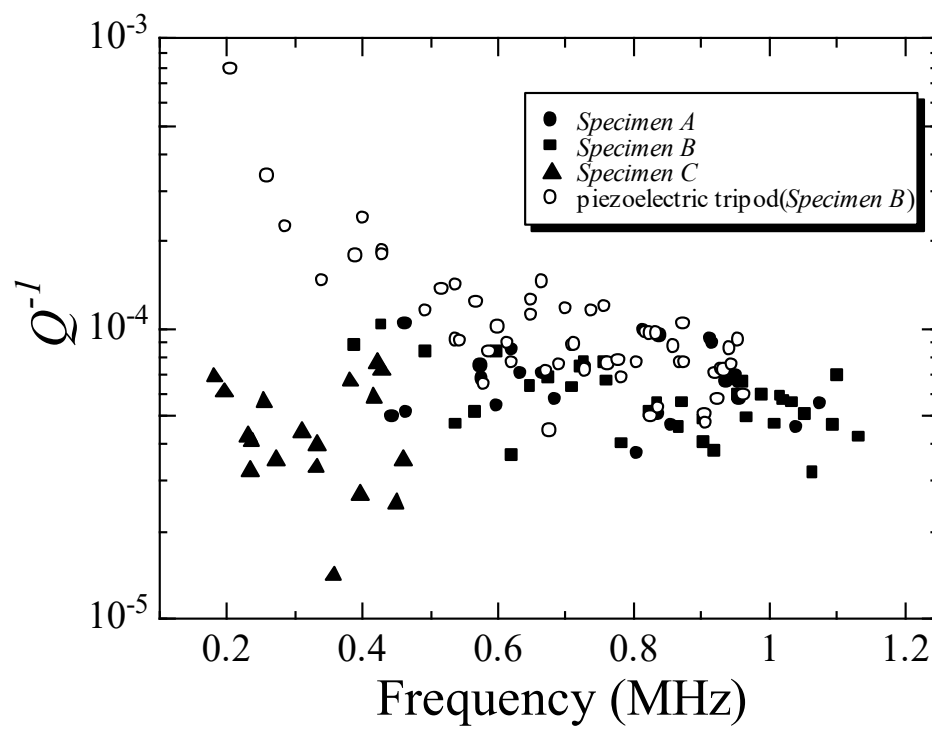(c) B_u-12 (321 kHz)

(d) B_g-12 (345 kHz)

Fig. 5

Fig. 6

Fig. 7